Supplementary Information

Efficient Nanoclay-Based Composite Photocatalyst: the Role of Nanoclay in Photogenerated Charge Separation

Denghui Jiang[a], Ziran Liu[b], Liangjie Fu[a,c], Huihua Jing[d], Huaming Yang[*,a,c,e]

[a] *Centre for Mineral Materials, School of Minerals Processing and Bioengineering, Central South University, Changsha 410083, China*

[b] *Department of Physics, Key Lab for Low-Dimensional Structures and Quantum Manipulation (Ministry of Education), Hunan Normal University, Changsha 410081, China*

[c] *Hunan Key Lab of Mineral Materials and Application, Central South University, Changsha 410083, China*

[d] *Hunan Institute of Food Quality Supervision Inspection and Research, Changsha 410111, China*

[e] *Key Lab of Clay Mineral Functional Materials in China Building Materials Industry, Central South University, Changsha 410083, China*

[*]*Corresponding author, Email: hmyang@csu.edu.cn, Fax: 86-731-88710804, Tel.: 86-731-88830549*

Table S1 Data fitting using a Langmuir-Hinshelwood model and reaction rate constant for photo-degradation of MO in the presence of different samples

Samples	*K* (min^{-1})	Standard Error	R^2
CdS	0.0232	0.0012	0.9837
CdS+Kaol	0.0708	0.0052	0.9737
CdS/Kaol	0.1044	0.0148	0.9424
CdS+Kaol-550	0.0283	0.0008	0.9948
CdS/Kaol-550	0.0469	0.0088	0.8220

Table S2 Apparent quantum efficiencies of different samples

Samples	*K* (min^{-1})	T %	I = 1 - T %	S	$\Phi = K/S*I$
CdS	0.0232	8.3 %	0.917	44.12	$0.57*10^{-3}$
CdS+Kaol	0.0708	2.4 %	0.976	45.50	$1.59*10^{-3}$
CdS/Kaol	0.1044	2.5 %	0.975	51.65	$2.07*10^{-3}$

Apparent quantum efficiency was defined as[1-2]:

$$\Phi = K / \alpha * I \quad (1)$$

where K is the photodegradation rate of MO, T is the transmittance of suspension under visible light irradiance. S is areas for the convolution of the irradiance of the light source with the UV–vis diffuse reflection spectrum of the samples at $400 \leq \lambda \leq 600$ nm. I is total optical power irradiance at the sample, which includes light scattering and light absorbed by the samples. In our experiments, CdS/Kaol-2 and CdS/Kaol-3 had similar photodegradation rate (Fig. S5), suggesting a negative effect of Kaol NSs in photodegradation. This result also indicates the shielding effect of Kaol NSs is stronger than that of light scattering enhancement for CdS nanoparticles. Hence, the apparent quantum efficiency of CdS/Kaol is underestimated, compared with pure CdS.

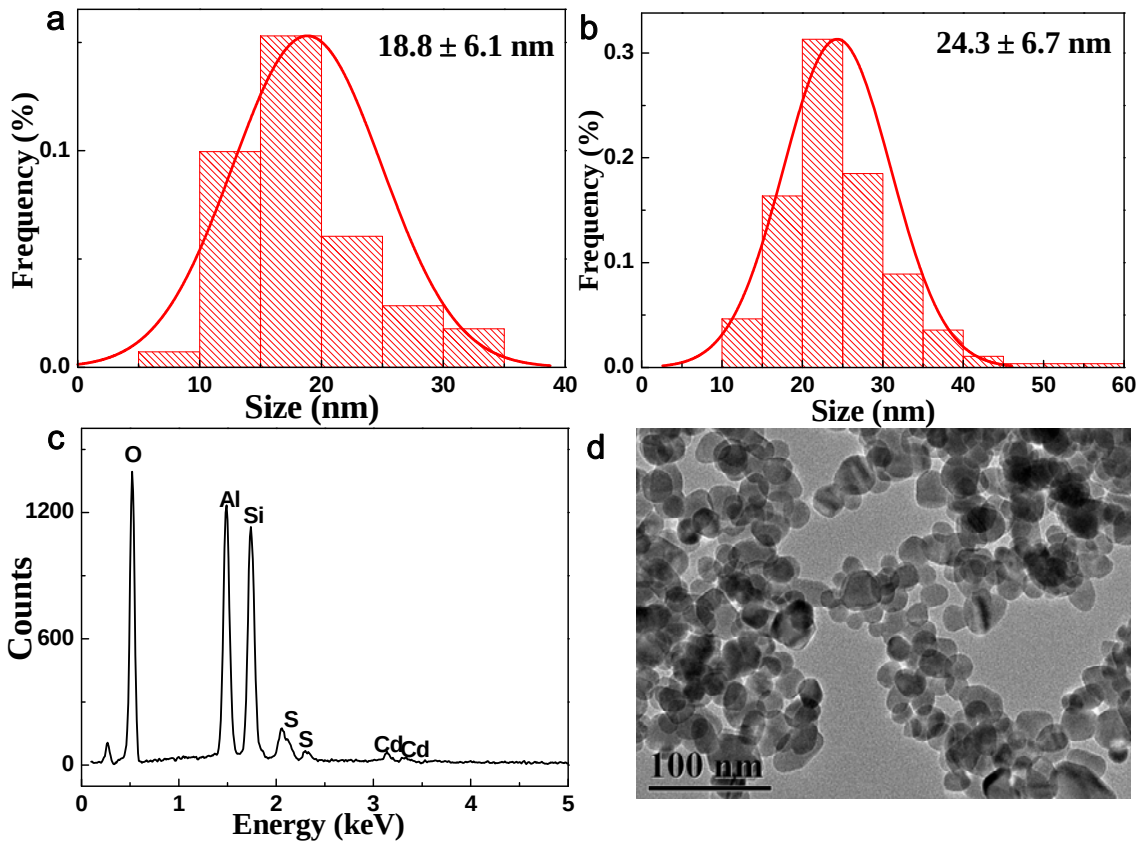

Figure S1. Size distribution histograms and standard deviations of (a) CdS nanoparticles in CdS/Kaol composites and (b) pure CdS nanoparticles, the corresponding EDX analysis of (c) CdS/Kaol composites and (d) TEM image of pure CdS nanoparticles.

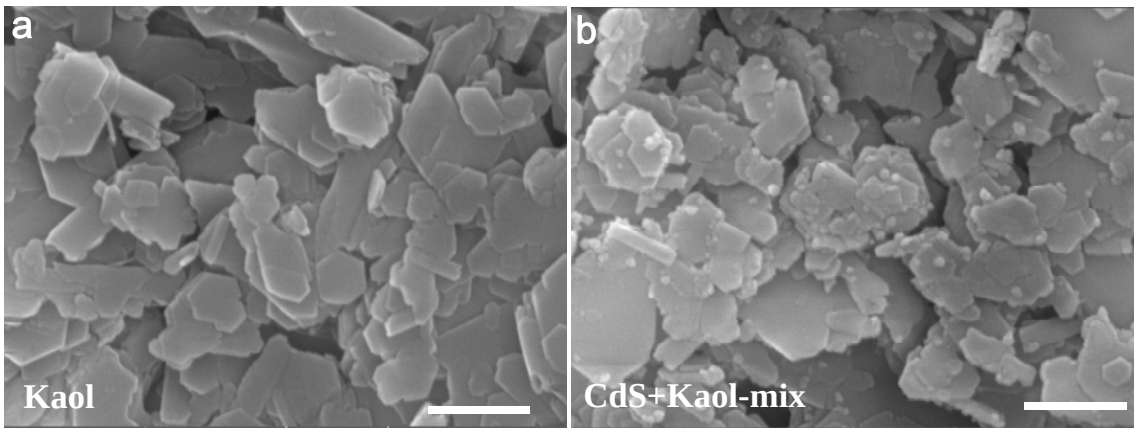

Figure S2. SEM images of (a) Kaol and (b) CdS+Kaol-mix. Scale bar = 500 nm.

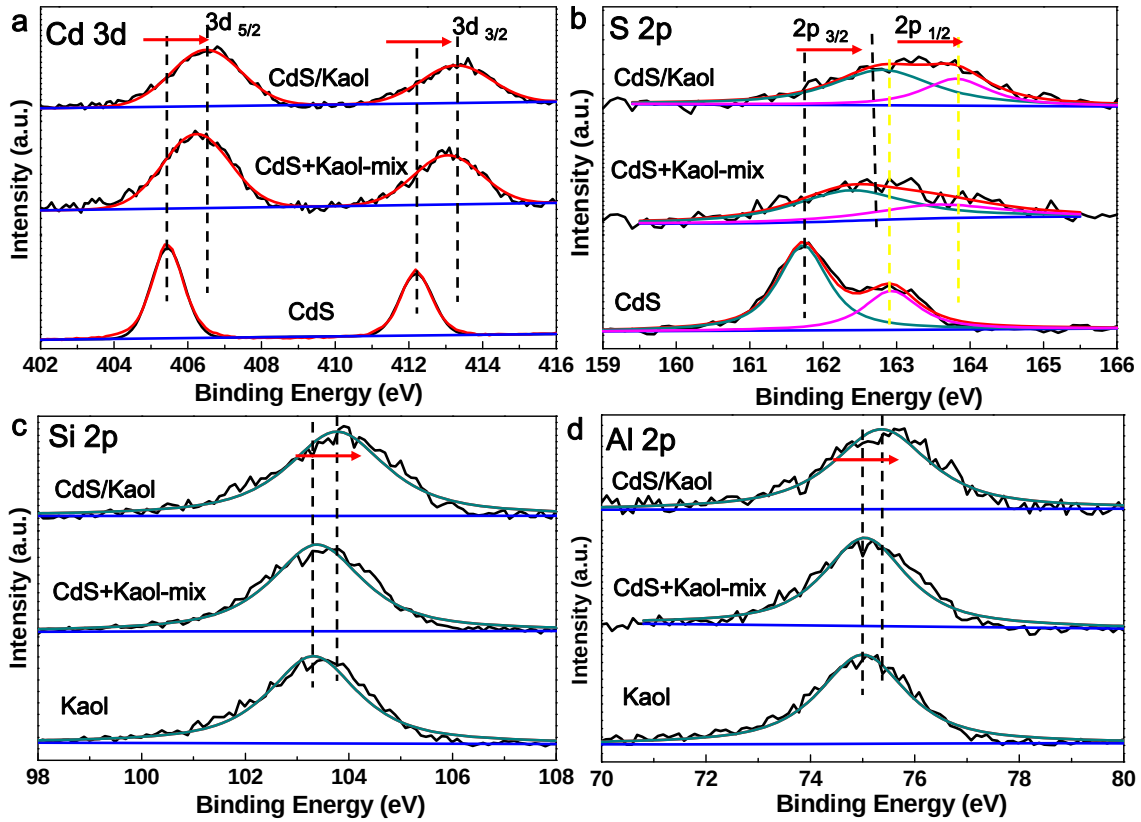

Figure S3. XPS spectra of (a) Cd 3d, (b) S 2p, (c) Si 2p and (d) Al 2p for different samples, respectively.

In the Al 2p and Si 2p spectra of XPS (Fig. S3c and S3d), the peaks of CdS+Kaol-mix samples had no obvious shift while that of CdS/Kaol composite had a significant shift to high energy direction compared to pure kaolinite clay. Thus, we inferred that the shifts of Al 2p and Si 2p spectra in CdS/Kaol were attributed to effects of hydrothermal process and the XPS charging effects, due to the changes of structure and surface state of Kaol NSs induced by hydrothermal process and the lower conductivity of Kaol NSs.

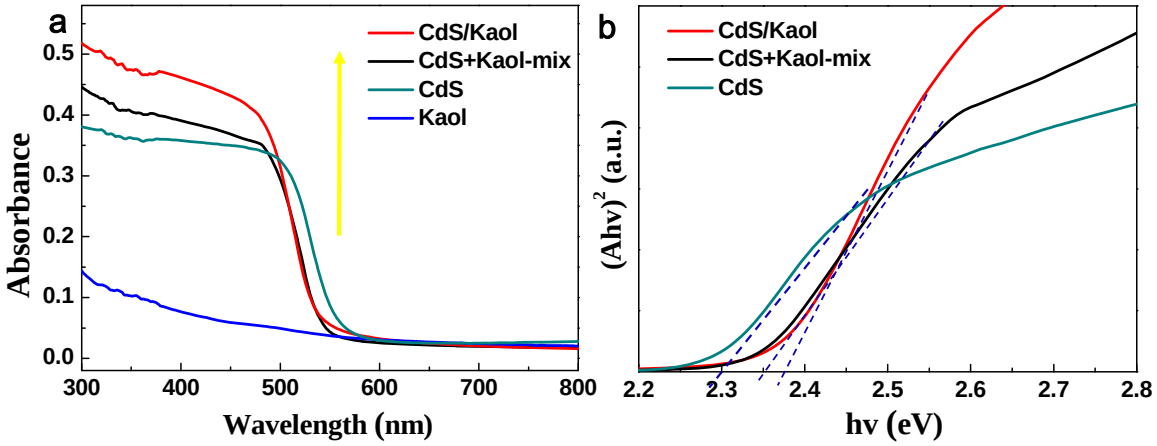

Figure S4. (a) UV–vis diffuse reflection spectrum and (b) Ahv–hv curve of CdS/Kaol, CdS+Kaol-mix and pure CdS nanoparticles (A is absorbance).

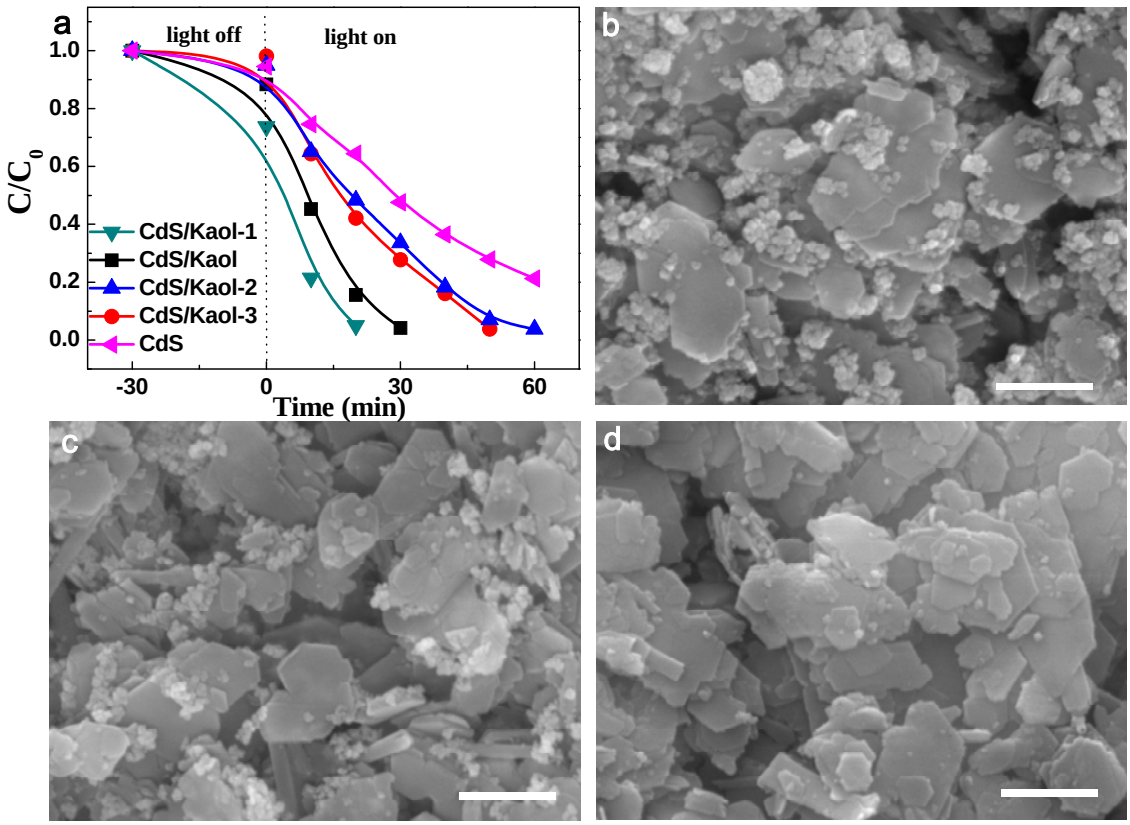

Figure S5. (a) Photodegradation rate of CdS/Kaol samples prepared at different content of Kaol, and SEM images of (b) CdS/Kaol-3, (c) CdS/Kaol-2 and (d) CdS/Kaol-1, respectively. **Scale bar** = 500 nm.

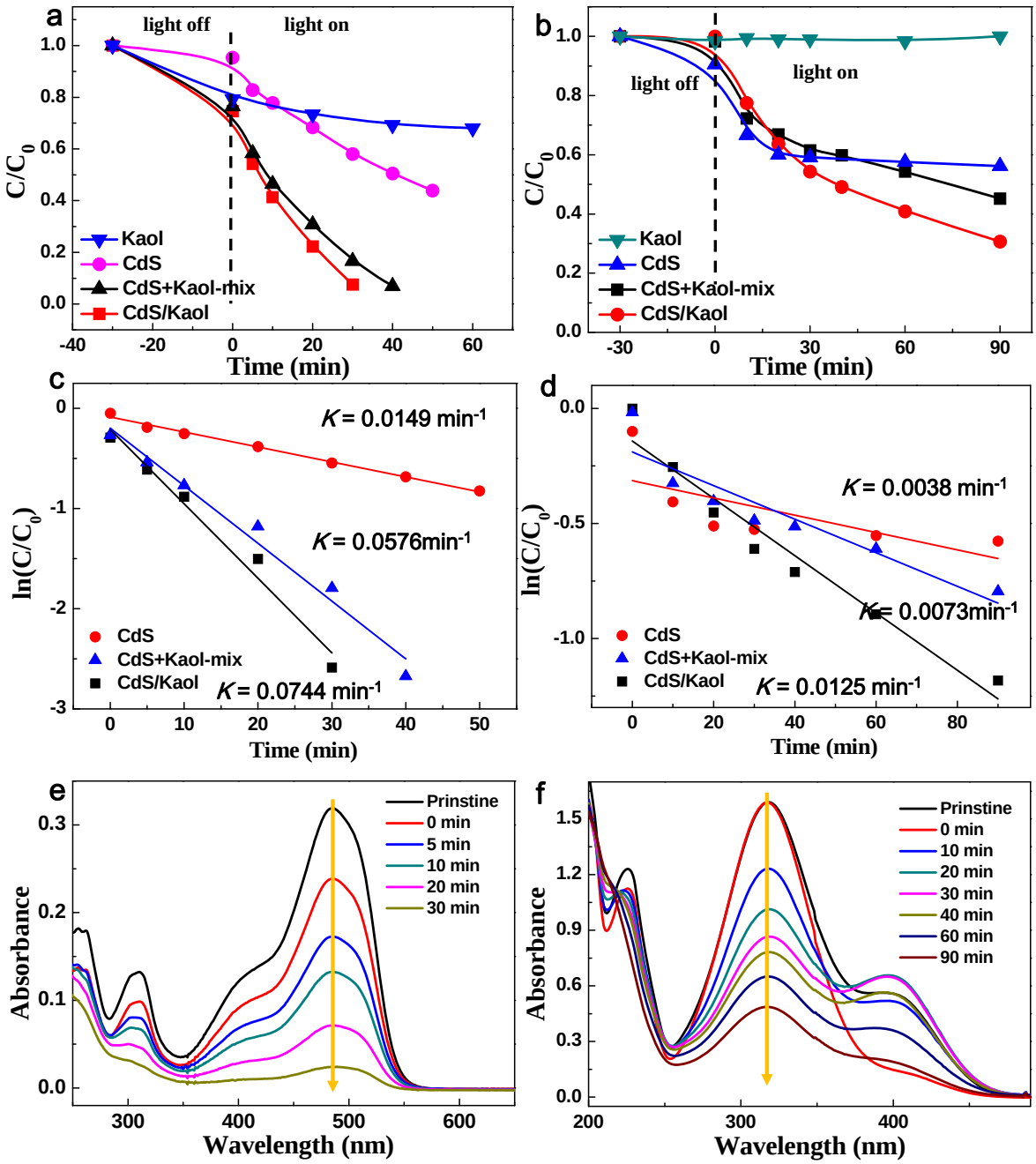

Figure S6. Photodegradation curves of Orange II (a) and 4-NP (b) in present of different samples, intrinsic photodegradation rates for Orange II (c) and 4-NP (d) degradation and time-dependent absorption spectra of Orange II (e) and 4-NP (f) photodegradation solutions in present of CdS/Kaol samples under the same photodegradation conditions of MO (50ml, 2×10^{-5} M).

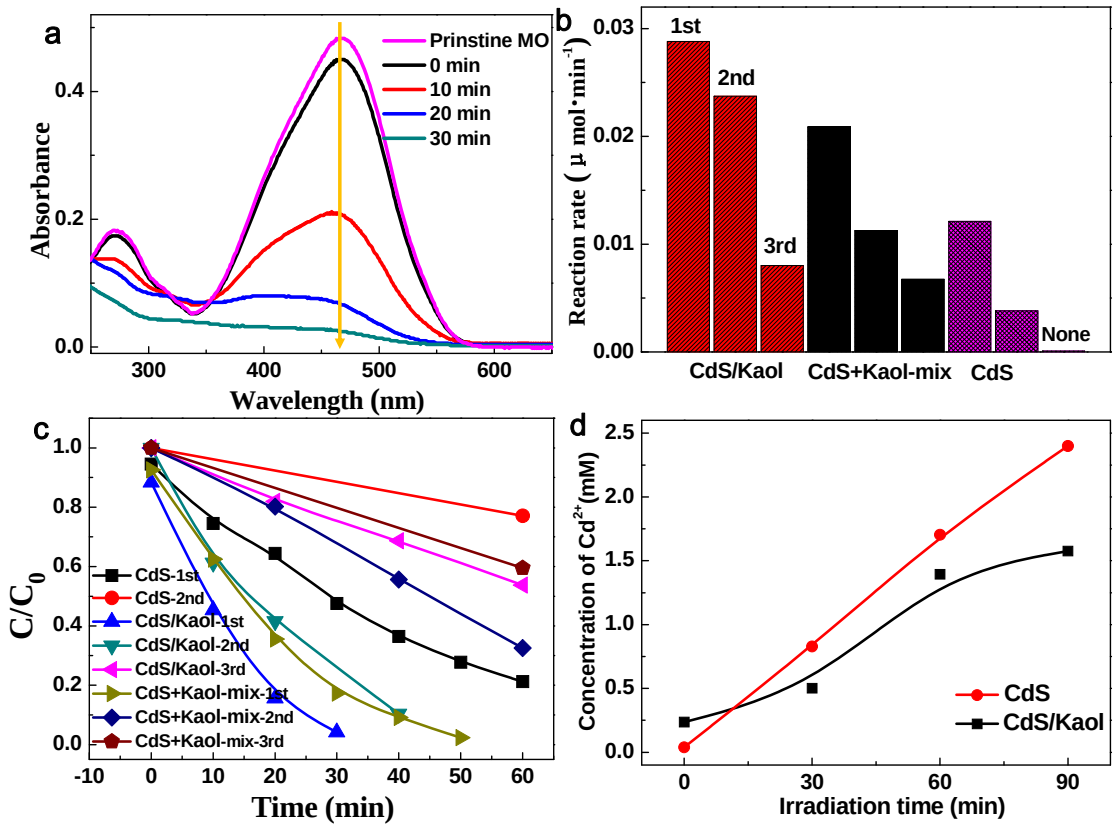

Figure S7. (a) Time-dependent absorption spectra of MO photodegradation solutions in present of CdS/Kaol samples, (b) photocatalytic stability comparison and (c) cyclic photodegradation curves of CdS/Kaol, CdS+Kaol-mix and CdS. (d) The cadmium ion concentration change of photodegraded reaction solution using CdS/Kaol and pure CdS nanoparticles as photocatalysts, respectively.

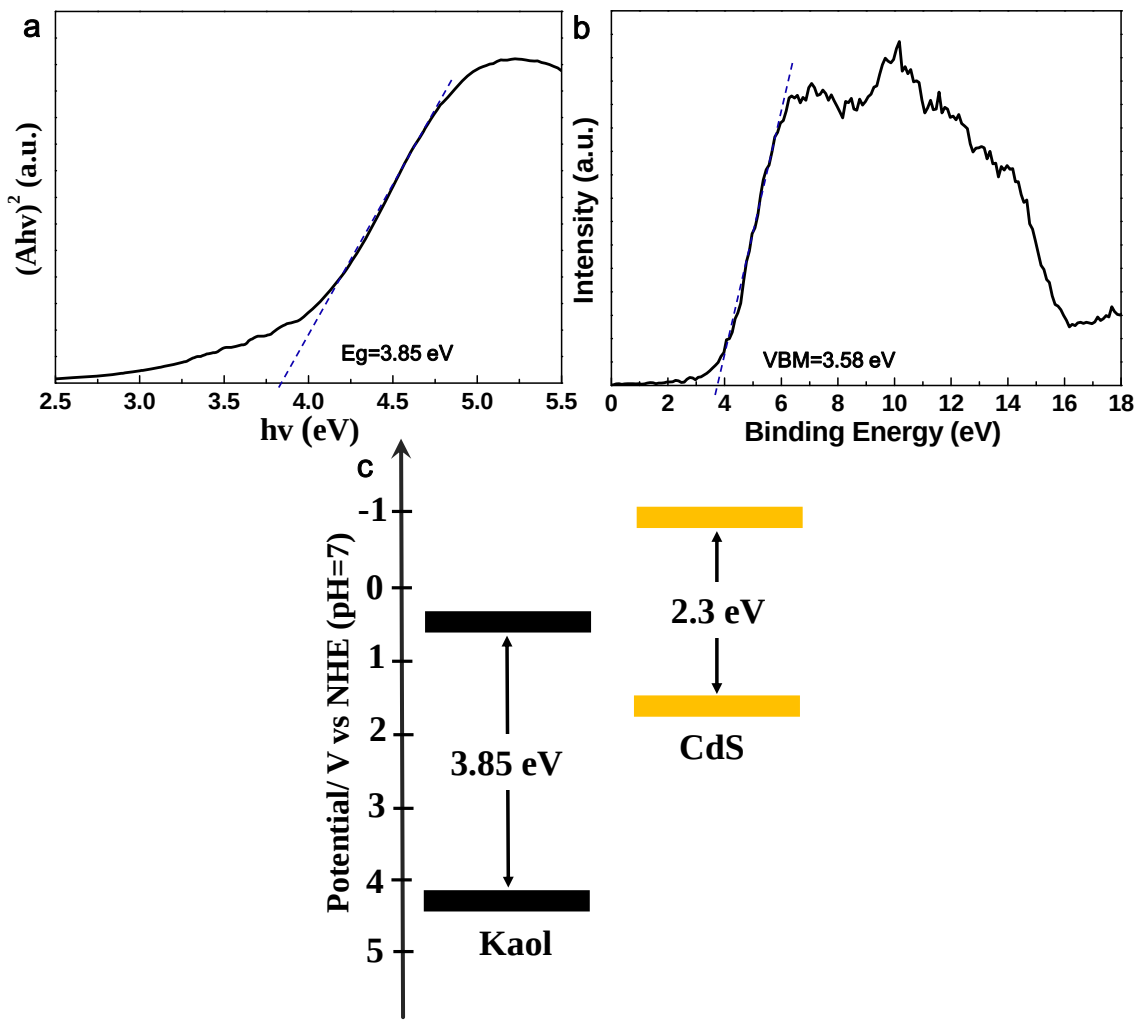

Figure S8. (a) Ahν–hν curve, (b) XPS valence band spectra and (c) band structure alignments of Kaol (A is absorbance).

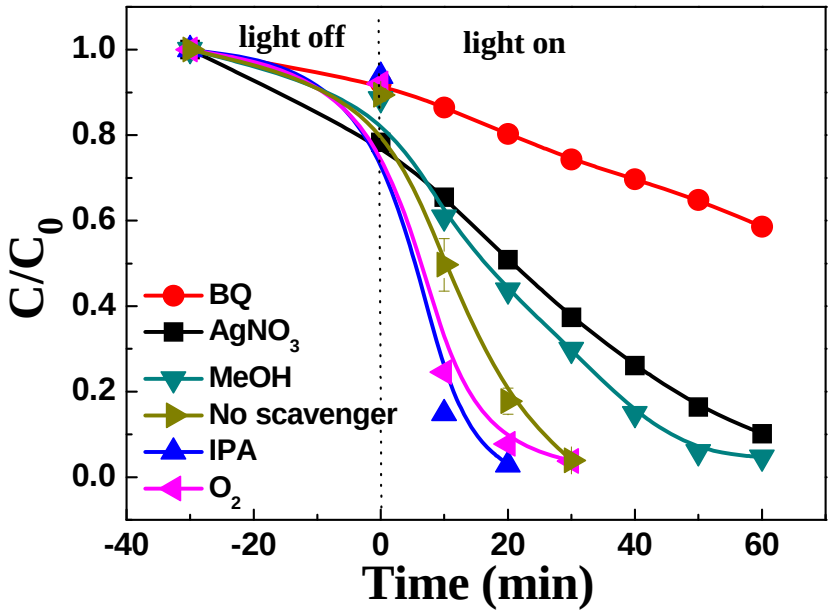

Figure S9. Effects of various scavengers on the photocatalytic activity of CdS/Kaol in the MO degradation. 0.54 mg of BQ, 8.5 mg of $AgNO_3$, 1.6 g of MeOH and 3 g of IPA were added in photocatalytic reaction systems, respectively.

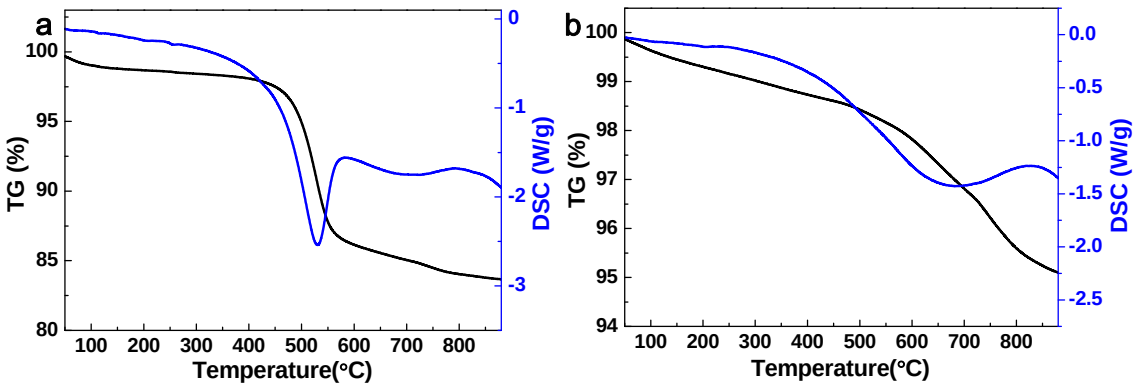

Figure S10. DSC and TG curves of (a) raw kaolinite and (b) kaolinite calcined at 550 °C.

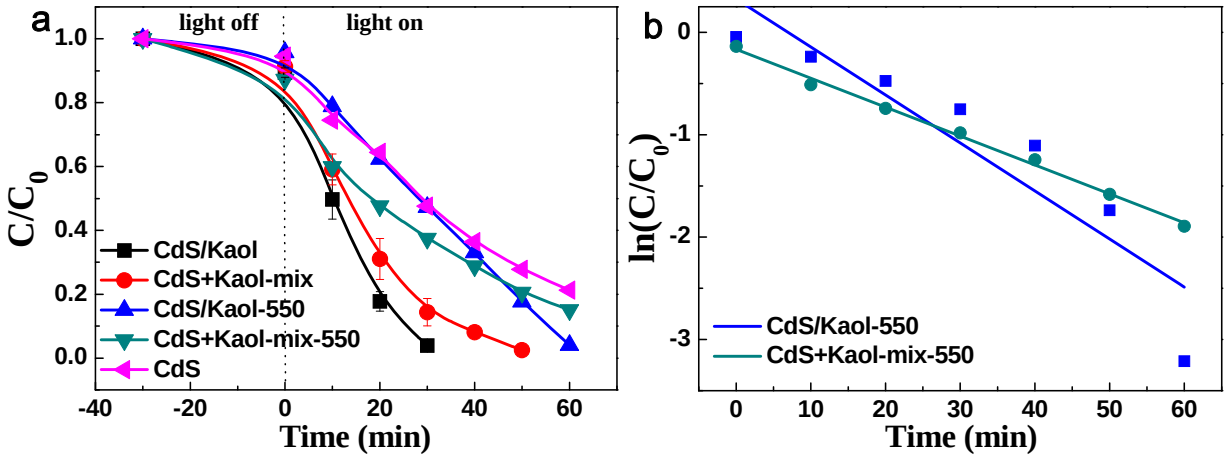

Figure S11. (a) Photocatalytic activities and (b) intrinsic photodegradation rates for MO degradation of CdS/Kaol-550 and CdS+Kaol-mix-550.

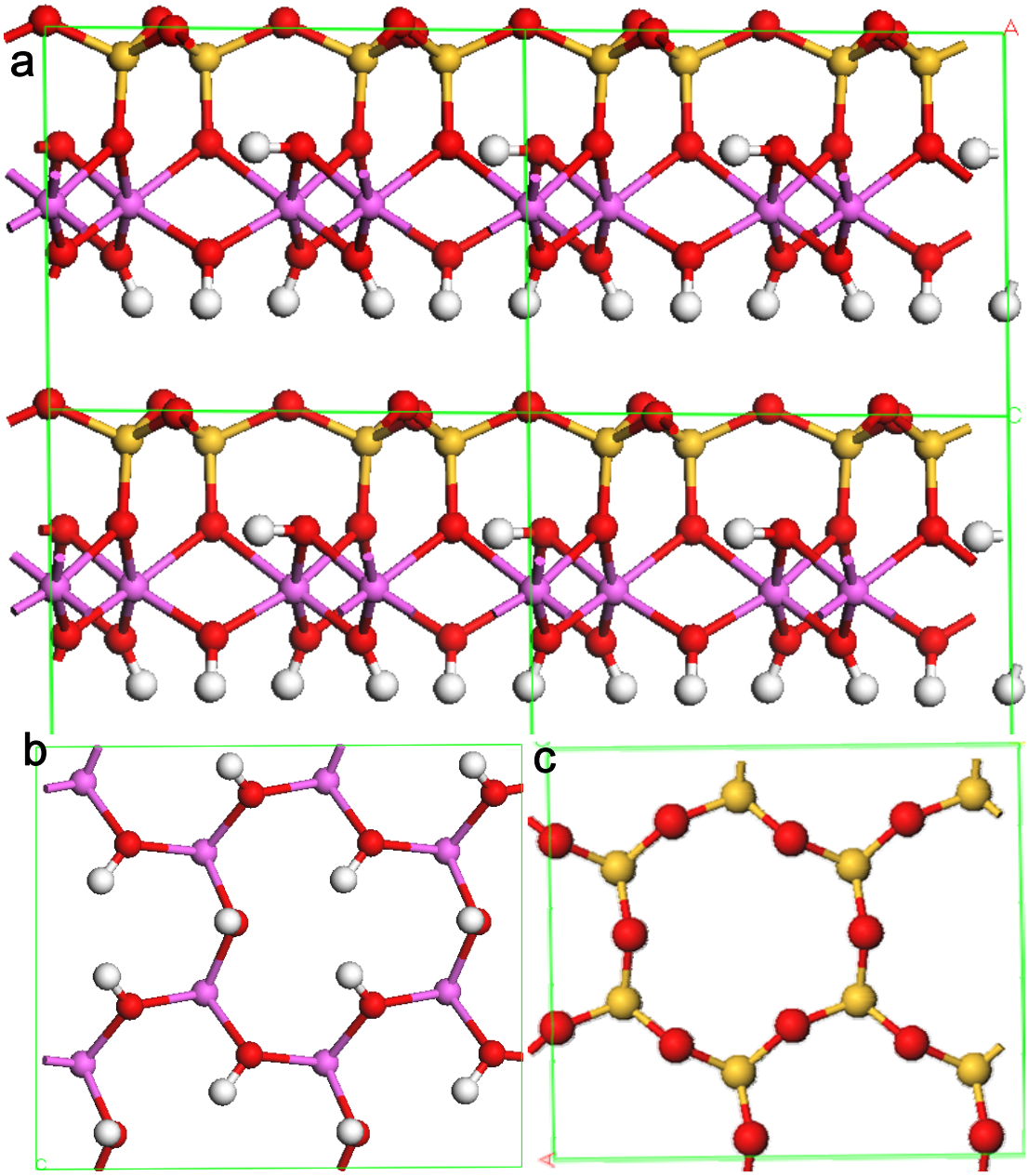

Figure S12. Crystal structure of (a) bulk kaolinite, (b) top view of (001) surface and (c) (00-1) surface. Only the topmost atoms are shown in the graphs. The purple, yellow, red and white balls represent Al, Si, O and H atoms, respectively.

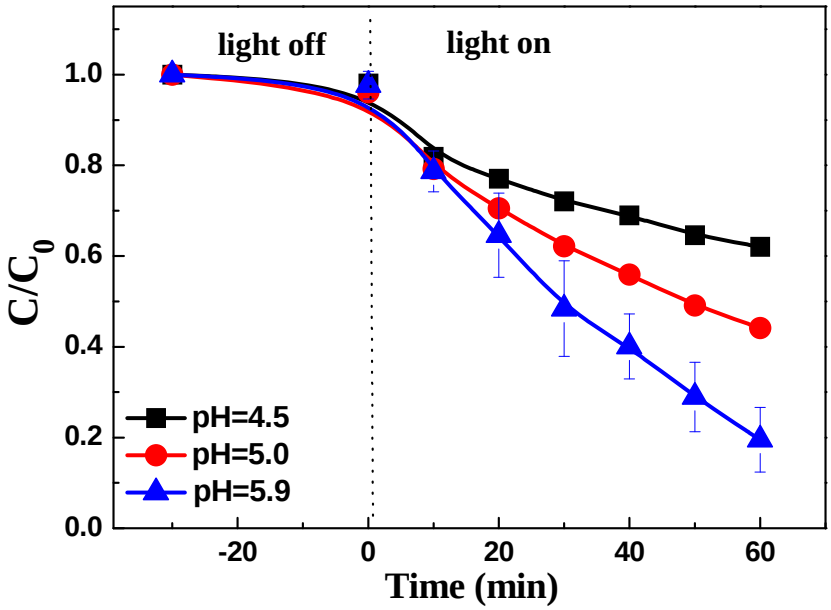

Figure S13. Photocatalytic abilities of CdS nanoparticles in different pH.

REFERENCES:

(1) Buriak, J. M.; Kamat, P. V.; Schanze, K. S. Best Practices for Reporting on Heterogeneous Photocatalysis. *ACS Appl. Mat. Interfaces* **2014**, *6*, 11815-11816.

(2) Aguirre, M. E.; Zhou, R.; Eugene, A. J.; Guzman, M. I.; Grela, M. A. Cu_2O/TiO_2 Heterostructures for CO_2 Reduction Through a Direct Z-Scheme: Protecting Cu_2O from Photocorrosion. *Appl. Catal., B* **2017**, *217*, 485-493.